Ratiometric paramagnetic probe based on ABTS$^{•+}$ and Mn^{2+} for detection of glutathione and revelation of the mechanism for MnO$_2$ nanosheet induced oxidation of ABTS

Hui Shi [a],[1], Li Tang [a],[1], Chunyu Wang [b], Zhimin Zhang [a], Meijun Lu [a], Daqian Song [a], Ziwei Zhang [a],[*]

[a] *College of Chemistry, Jilin Province Research Center for Engineering and Technology of Spectral Analytical Instruments, Jilin University, Qianjin Street 2699, Changchun 130012, PR China*
[b] *State Key Laboratory of Supramolecular Structure and Materials, Jilin University, Qianjin Street 2699, Changchun 130012, PR China*

ARTICLE INFO

ABSTRACT

We designed a ratiometric paramagnetic probe based on electron spin resonance (ESR) signals of ABTS radical (ABTS$^{•+}$) and Mn^{2+}. Two ESR signals from different paramagnetic species (ABTS$^{•+}$ and Mn^{2+}) coexisting in the same solution were measured at the same time and were present in one spectrum. MnO$_2$ nanosheets with oxidase-like properties were synthesized. The probe was used to investigate the oxidation mechanism of ABTS by MnO$_2$ nanosheets. On one hand, MnO$_2$ nanosheets catalyzed the generation of O$_2^{•-}$ which oxidized ABTS to ABTS$^{•+}$, and on the other hand, a small amount of ABTS was directly oxidized to ABTS$^{•+}$ by MnO$_2$ which was reduced to Mn^{2+}. Glutathione (GSH) underwent a redox reaction with MnO$_2$ nanosheets to yield Mn^{2+} with stable ESR signal. The concentration of MnO$_2$ decreased in the presence of GSH, which inhibited the production of O$_2^{•-}$ and ABTS$^{•+}$. As a result, as the concentration of GSH increased, ESR signal of ABTS$^{•+}$ descended and on the contrary ESR signal of Mn^{2+} ascended. Accordingly, the signal ratio of ABTS$^{•+}$ to Mn^{2+} decreased with the increase of GSH concentration. The proposed ratiometric ESR probe could reduce the influence from background signal and improve the accuracy and sensitivity of the detection. We applied this strategy to the determination of GSH in human erythrocyte cells, and the results showed recoveries between 90.9 % and 92.6 %. With this method, simultaneously monitoring both nanozyme and its chromogenic substrate could be realized and thus a better understand of the mechanism for the function of MnO$_2$ nanomaterial could be achieved.

1. Introduction

Glutathione (GSH) is a non-protein thiol composed of glycine, cysteine and glutamate, which belongs to the tripeptide class and has strong reducing properties. It mainly exists in two states, reduced form (GSH) and oxidized form (GSSG), which can be used to regulate the oxidation-reduction homeostasis of cells [1]. GSH also plays an important role in free radical scavenging, detoxification of xenobiotic, gene regulation and intracellular signal transduction[2,3]. Therefore, accurate detection of GSH content is of great practical significance. In recent years, researches have proposed a series of GSH detection methods, mainly including high performance liquid chromatography (HPLC) [4], fluorescence spectroscopy [5], colorimetry [6], mass spectrometry[7]

and electrochemistry [8]. Because of the major content of GSH relative to GSSG in biological samples as well as the reducing capability of GSH when reacting with MnO$_2$ nanomaterials, only the reduced form GSH was investigated in this work.

Natural enzymes are mostly proteins with high specificity and catalytic activity. Nevertheless, the intrinsic drawbacks of natural enzymes such as low stability, high cost and complex purification process greatly limit their practical application [9,10]. In recent years, a class of nanomaterials with enzyme-mimic properties has greatly attracted the interest of researchers. MnO$_2$ nanomaterials of various morphologies have been used as either oxidase or peroxidase mimic due to their simple synthesis process, low cost, easy storage and high oxidase or peroxidase mimetic activity [11]. For example, Liu et al. utilized the oxidase-like

---

activity of MnO_2 nanosheets to oxidize 3,3',5,5'-tetramethylbenzydine (TMB) into ox-TMB with blue color detected by colorimetry, and GSH is then indirectly determined based on the decomposition of MnO_2 nanosheets by GSH [12]. However, in most publications with respect to the oxidation reaction between MnO_2 nanomaterial and the chromogenic agent such as TMB, only the product i.e. the chromophore is detected and the change happen to MnO_2 nanomaterial is unknown.

2,2'-Azinobis (3-ethylbenzothiazoline-6-sulfonic acid ammonium salt) (ABTS) is a chemically synthesized chromogenic agent commonly used to detect enzyme activity and assess antioxidant capacity [13,14]. ABTS is oxidized to ABTS cationic radical ($ABTS^{\bullet+}$) by single-electron transfer and $ABTS^{\bullet+}$ has a stable electron spin resonance (ESR) signal. ESR spectroscopy can be used to detect paramagnetic substances with single electrons [15]. In this work, an analytical method for the determination of GSH by ESR spectroscopy based on the ESR signal ratio of $ABTS^{\bullet+}$ to Mn^{2+} has been established. Benefiting from the ESR technique for simultaneously monitoring both Mn^{2+} generated from MnO_2 nanomaterial and $ABTS^{\bullet+}$ radical as the product of the oxidation reaction, the mechanism for the oxidase mimetic role of MnO_2 nanomaterial can be better explored.

Herein, we proposed a novel ratiometric ESR probe, and the probe was utilized to explore the reaction mechanism between MnO_2 nanosheets and ABTS based on the simultaneous detection of $ABTS^{\bullet+}$ and Mn^{2+} in the same solution. GSH underwent a redox reaction with MnO_2 nanosheets and MnO_2 nanosheets were disintegrated into Mn^{2+}. At the same time, MnO_2 nanosheets with good oxidase-like activity catalyzed the production of superoxide radical from dissolved oxygen and the resulting superoxide radical can oxidize ABTS to $ABTS^{\bullet+}$ with stable ESR signal. Based on simultaneous detecting $ABTS^{\bullet+}$ and Mn^{2+} in the same sample, we successfully constructed a ratiometric ESR probe to develop a new method for determination of GSH and to explore the function of MnO_2 nanomaterial.

2. Materials and methods

2.1. Materials and apparatus

The materials and apparatus used are mentioned in Supplementary Material.

2.2. Synthesis of MnO_2 nanosheets

MnO_2 nanosheets were synthesized according to the previous publication [16]. 12 mL of 1 mol L^{-1} tetramethylammonium hydroxide (TMA·OH) and 2 mL of H_2O_2 (30 wt%) were first mixed to a total volume of 20 mL, and then the mixture was added into $MnCl_2$ solution (10 mL, 3 mmol L^{-1}) immediately. The resulting solution was stirred vigorously at room temperature for 12 h, washed alternately with methanol and distilled water and vacuum dried at 60 °C to obtain bulk MnO_2. The bulk MnO_2 was grounded to powder in a mortar. 200 mg of the powder were dissolved in 40 mL distilled water and then sonicated for 10 h. Finally, the supernatant was separated by centrifugation at 2000 rpm for 30 min and used as the nanosheet solution.

2.3. Study of oxidase-like activity of MnO_2 nanosheets

ABTS was used as the substrate to study the oxidase-like activity of MnO_2 nanosheets. Typically, 22.5 μL of MnO_2 nanosheets, 22.5 μL of ABTS and 22.5 μL of 4-(2-hydroxyethyl)-1-piperazineethanesulfonic acid (HEPES) (100 mmol L^{-1}, pH 5.0) were mixed and diluted to 450 μL with distilled water. The concentrations of MnO_2 nanosheets and ABTS in the resulting solution were respectively 0.004 mg mL^{-1} and 0.5 mmol L^{-1}. The mixture solution was reacted at room temperature for 20 min before ultraviolet-visible (UV–vis) measurement at 734 nm.

2.4. Steady-state kinetic analysis of MnO_2 nanosheets as oxidase mimic

Steady-state kinetic experiments were performed in HEPES buffer (100 mmol L^{-1}, pH 5.0) consisting of 0.004 mg mL^{-1} MnO_2 nanosheets and a series concentrations (0.05–0.75 mmol L^{-1}) of ABTS. The initial velocity (v) of the catalytic reaction was measured within the 1st min after the start of the reaction. The dynamic parameters were determined in accordance with the Michaelis-Menten equation: $v=V_{max}[S]/(K_m+[S])$, where v and V_{max} represent the initial velocity and the maximum velocity of the catalytic reaction, respectively; $[S]$ represents the substrate concentration; K_m represents the Michael-Menten constant.

2.5. Spin trapping ESR test

Both 5,5-dimethyl-1-pyrroline N-oxide (DMPO) and MnO_2 nanosheets were diluted with methanol and then mixed together to concentrations of 50 mmol L^{-1} and 0.02 mg mL^{-1}, respectively. The resulting solution was reacted for 5 min at room temperature and tested by ESR spectrometer. The instrumental parameters were set as follows: sweep width 80 Gauss, modulation amplitude 1.0 Gauss, microwave power 20 mW.

2.6. GSH detection

50 μL of MnO_2 nanosheets and 50 μL of various concentrations of GSH standard solution or sample solution were mixed homogeneously, and then 50 μL of ABTS and 50 μL of HEPES (100 mmol L^{-1}, pH 6.0) were added. The concentrations of MnO_2 nanosheets and ABTS in the resulting solution were respectively 0.02 mg mL^{-1} and 2.5 mmol L^{-1}. The mixture solution was reacted for 20 min at room temperature to get an analytical sample. Subsequently, the ESR spectrum of the analytical sample was collected.

2.7. Sample analysis with ESR spectrometer

15 μL of the analytical sample was injected into a glass capillary (0.8 mm inner diameter), and then the glass capillary was placed into a quartz tube (4 mm diameter), and finally the quartz tube was placed into the resonant cavity of the spectrometer. All ESR spectra were collected at room temperature, and three parallel samples were measured at each data point. In order to improve the repeatability of parallel experiments, when changing samples, the quartz tube was kept in the resonant cavity and only the glass capillary was replaced with the help of a long plastic tube attached to the top of the capillary. The instrumental parameters were set as follows: center magnetic field 3355 Gauss, sweep width 670 Gauss, modulation amplitude 4.0 Gauss, modulation frequency 100 kHz, microwave power 2 mW.

2.8. Real sample preparation

GSH was determined in human erythrocyte cells. Erythrocytes were separated from the whole blood by centrifugation at 1500 g for 15 min and removal of serum. 500 μL of erythrocytes were gathered and washed with phosphate buffered saline (PBS) for three times until the plasma was removed completely. Then the erythrocytes were hemolyzed by adding distilled water (3:1, v/v) and incubating the mixture on ice for 20 min. After centrifugation at 8000 g for 5 min, the supernatant was collected, filtered through a Microsep 3 K membrane and diluted twice with distilled water. The resulting solution was used as sample solution for the determination of GSH.
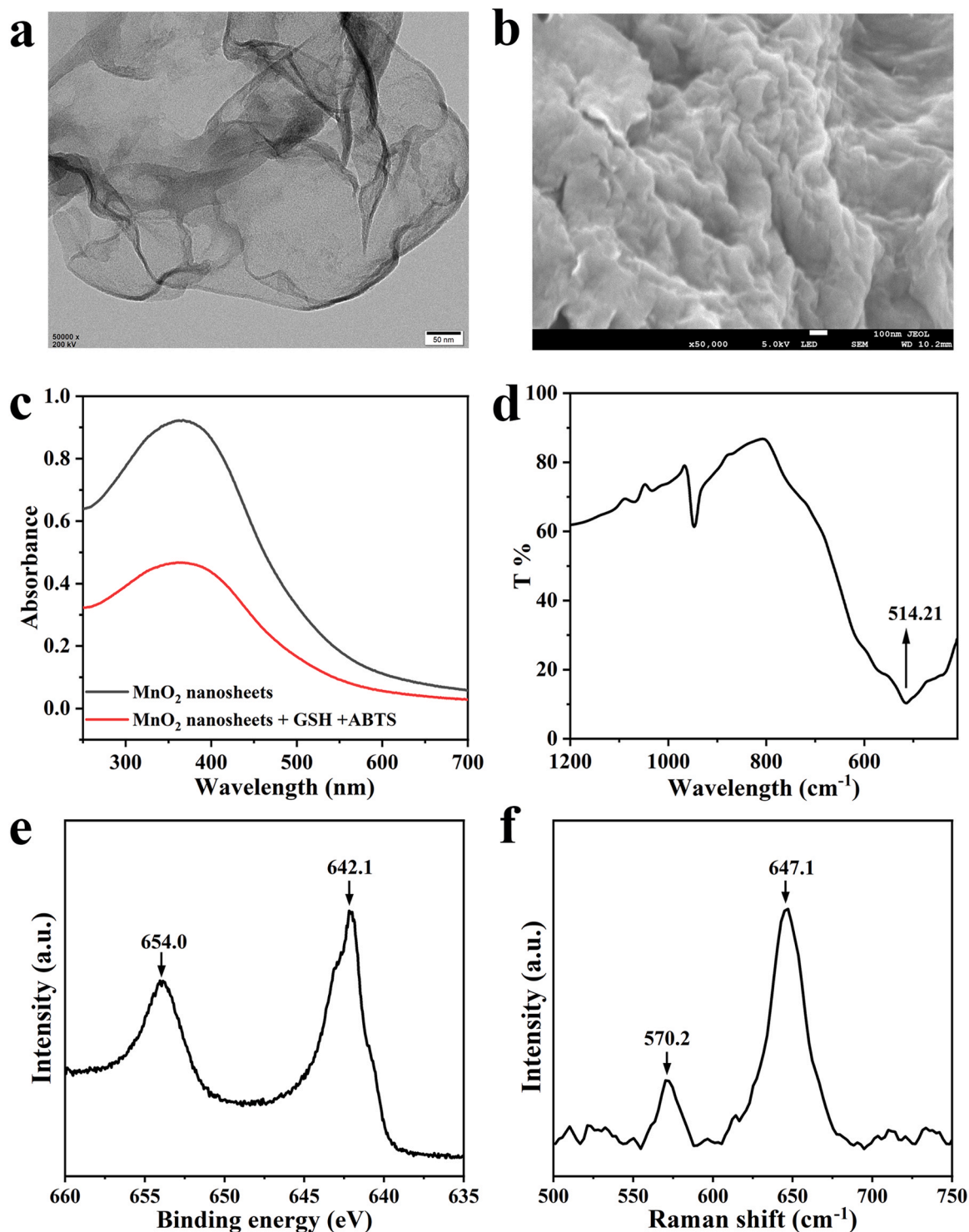
Fig. 1. TEM image (a), SEM image (b), UV–vis spectra (c), FT-IR spectrum (d), XPS spectrum (e) and Raman spectrum (f) of MnO_2 nanosheets.

3. Results and discussion

3.1. Characterization of MnO_2 nanosheets

The morphology of MnO_2 nanosheets was observed through transmission electron microscope (TEM) (Fig. 1a) and scanning electron microscope (SEM) (Fig. 1b), showing a typical two-dimensional morphology with unique sheet-like structure and folds. The UV–vis spectrum (the black line in Fig. 1c) indicates that MnO_2 nanosheets had a wide absorption band between 250 and 700 nm. When GSH coexisted with the nanosheets, the UV–vis absorption (the red line in Fig. 1c) dramatically decreased due to a breakdown of the nanostructure caused by the reducing action of GSH. In the Fourier transform infrared (FT-IR) spectrum of MnO_2 nanosheets, Mn-O bond was observed around 514 cm^{-1} (Fig. 1d). The X-ray photoelectron spectroscopy (XPS) spectrum of MnO_2 nanosheets is shown in Fig. 1e. Two peaks at 654.0 and 642.1 eV belong to the $Mn_{2p1/2}$ and $Mn_{2p3/2}$, respectively. The Raman shift centered at 570.2 and 647.1 cm^{-1} in Fig. 1f can be contributed to the Mn-O vibration. The X-ray diffraction (XRD) pattern of MnO_2 nanosheet powder is displayed in Figure S1. Four broad peaks at 9.2°,
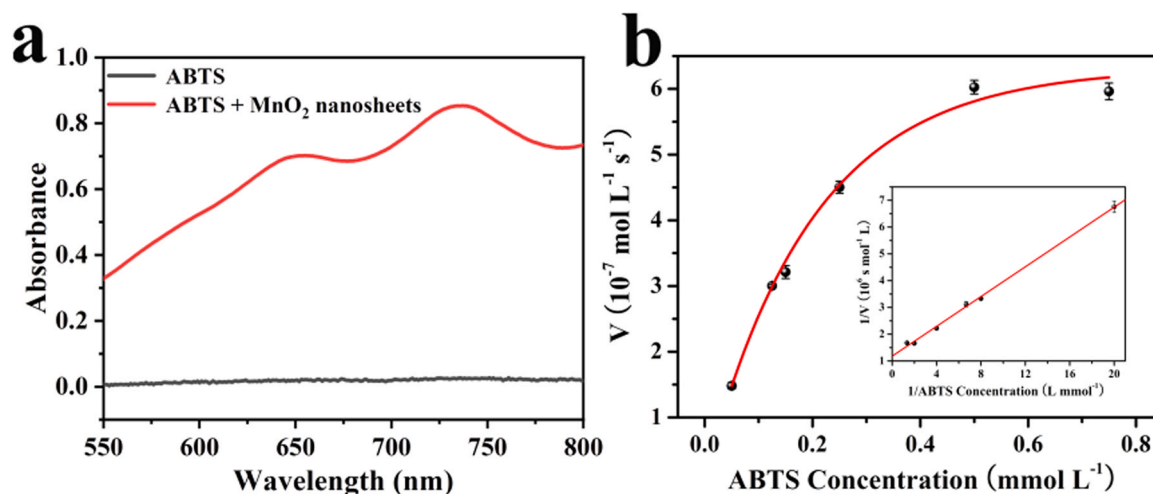
Fig. 2. (a) UV–vis spectra of ABTS in the absence (black line) and in the presence of MnO$_2$ nanosheets (red line); (b) Michaelis-Menten curve of MnO$_2$ nanosheets towards ABTS as the substrate. Inset shows Lineweaver-Buck double reciprocal plot and its linear fit. The error bar represents standard deviation (SD).

18.4°, 36.4° and 65.1° indexed as (001), (002), (100), (110) were observed, indicating the poor crystallinity of MnO$_2$ nanosheets [12,17]. These characterization results are consistent with those reported in the literature [18–20], demonstrating the successful synthesis of MnO$_2$ nanosheets.

3.2. Oxidase-like activity of MnO$_2$ nanosheets

Using ABTS as the substrate, the catalytic activity of MnO$_2$ nanosheets as oxidase mimic was investigated. When MnO$_2$ nanosheets were not added, ABTS was not oxidized and thus there was no UV–vis absorption (Fig. 2a, black line). However, when MnO$_2$ nanosheets were
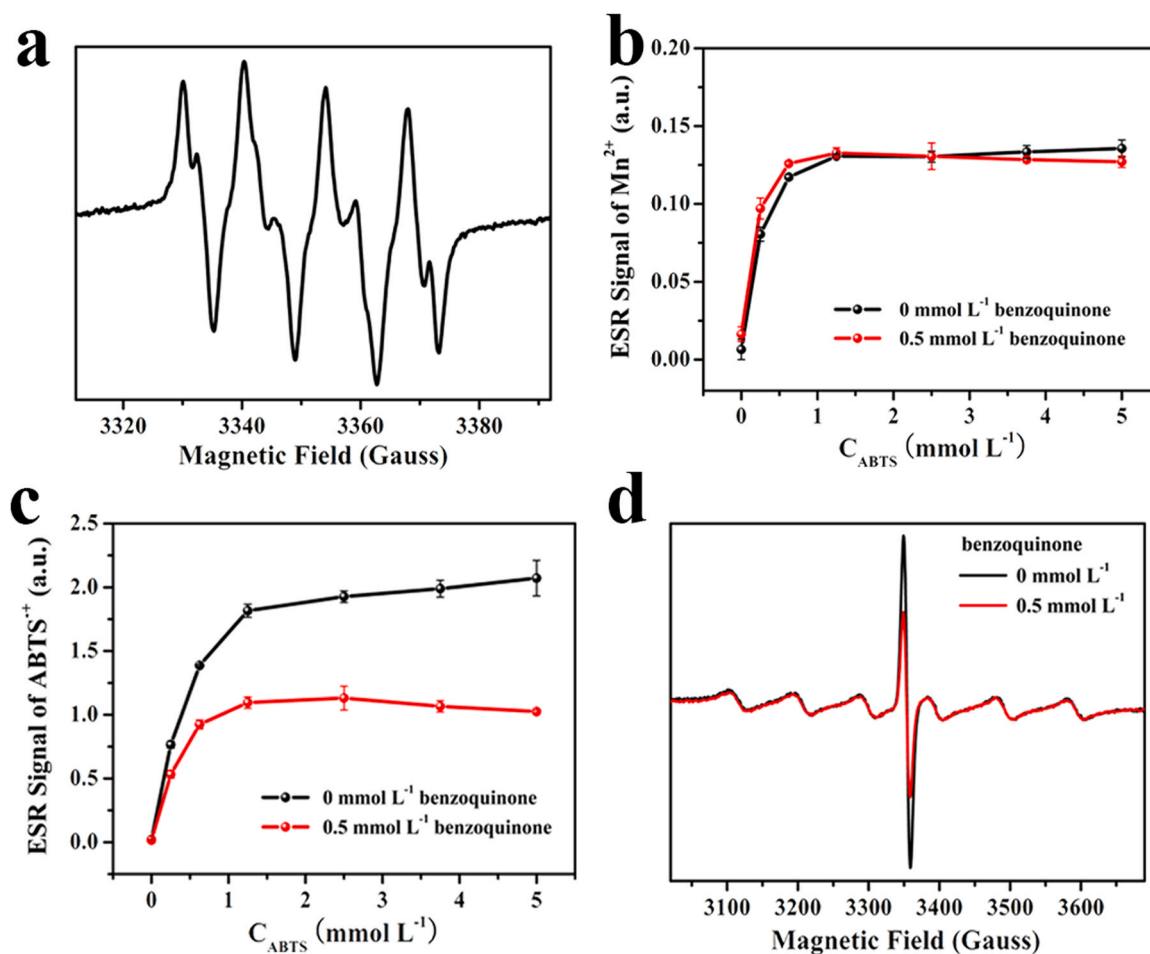

Fig. 3. (a) ESR spectrum of superoxide spin adduct observed using DMPO as the spin trapping agent; variation of ESR signals of Mn^{2+} (b) and ABTS$^{\bullet+}$ (c) with ABTS concentration in the absence and presence of benzoquinone; (d) ESR spectra in the absence and presence of benzoquinone. The error bar represents SD.

present, ABTS was oxidized to ABTS$^{\bullet+}$ and its characteristic UV–vis absorption peak at 734 nm appeared (Fig. 2a, red line). Similar to natural enzymes, oxidase-like activity of MnO$_2$ nanosheets is also affected by pH and temperature. As shown in Figure S2a, the oxidase-like activity of MnO$_2$ nanosheets almost did not change with temperate in the range of 15–35 °C. As seen in Figure S2b, the oxidase-like activity of MnO$_2$ nanosheets decreased slowly when pH increased from 5.0 to 6.0, and then decreased significantly when pH was higher than 6.0. Therefore, at 25 °C and pH 5.0, the oxidase-like activity of MnO$_2$ nanosheets was maximal.

To further understand the oxidase-like activity of MnO$_2$ nanosheets, steady-state kinetic experiments were performed using ABTS as the substrate. According to Michaelis-Menten curve (Fig. 2b) and the linear fit of Lineweaver-Buck double reciprocal plot (inset of Fig. 2b), the values for the Michael-Menten constant (K_m) and the maximum reaction velocity (V_{max}) were derived to be 0.236 mmol L^{-1} and 8.47×10^{-7} mol L^{-1} s^{-1}, respectively. The extinction coefficient of ABTS$^{\bullet+}$ in water at 734 nm (1.5×10^4 mol^{-1} L cm^{-1}) has been used in the calculation [21]. K_m represents the enzyme's affinity towards the substrate, and a smaller K_m value indicates a greater affinity towards the substrate. A comparison of the kinetic parameters with reported oxidase-mimic nanoenzymes as well as the natural oxidase laccase is listed in Table S1. In Table S1, most nanoenzymes use TMB as the substrate and laccase uses epinephrine as the substrate, whereas our result supplied kinetic data for ABTS as the substrate. MnO$_2$ nanosheets have a comparable K_m to that of laccase (0.194 mmol L^{-1}) [22] and a higher V_{max} than that of laccase and most nanoenzymes. The experimental results indicated an efficient catalytic capability of MnO$_2$ nanosheets towards the oxidation of ABTS.

3.3. Mechanism for the reaction between MnO$_2$ nanosheets and ABTS

Similar to natural oxidases, nanozymes have been proved to have oxidase-like activity and can catalyze the production of a variety of reactive oxygen species (ROS) such as superoxide radical (O$_2^{\bullet-}$) and singlet oxygen (^{1}O$_2$) [23]. In order to investigate the oxidase-like property of MnO$_2$ nanosheets, spin trapping ESR test was performed. Fig. 3a shows an ESR spectrum obtained from spin trapping test in methanol with DMPO as the trapping agent. The spectrum had a broad quartet with the hyperfine splitting constants (hfsc) A_N=13.7 Gauss and A_H=10.2 Gauss, indicating the generation of superoxide (O$_2^{\bullet-}$) spin adduct. The broadening is caused by a high concentration of dissolved oxygen [24] and the hfsc values are consistent with superoxide spin adduct with DMPO in ethanol or methanol generated by CdS or phthalocyanine pigments [25] as well as superoxide spin adduct with DMPO in ethanol generated by irradiated TiO$_2$ [26]. Therefore, the generation of superoxide radical in the presence of MnO$_2$ nanosheets was proved and it could be a reason for the oxidation of ABTS. On the other hand, the standard redox potential of MnO$_2$/Mn^{2+} and ABTS$^{\bullet+}$/ABTS are respectively 1.23 V [27] and 0.68 V [28], suggesting that there is a possibility of redox reaction to occur between MnO$_2$ nanosheets and ABTS.

Then which is the dominant contribution to the oxidation of ABTS, the redox reaction or ROS by the catalysis of nanozyme? With respect to the oxidation of chromogenic substrates such as TMB and ABTS in the presence of MnO$_2$ nanomaterial, some publications believe that it is caused by the redox reaction between MnO$_2$ nanomaterial and the chromogenic substrate [27,29], whereas many other publications consider that it is caused by ROS generated by nanozyme-catalyzed reaction [30–32]. In this work, benefiting from simultaneous monitoring of ABTS$^{\bullet+}$ and Mn^{2+}, any change happen to both the chromogenic substrate and the nanomaterial could be monitored quantitatively at the same time. Thus a better understand of the mechanism for the interaction between MnO$_2$ nanomaterial and the chromogenic substrate could be achieved.

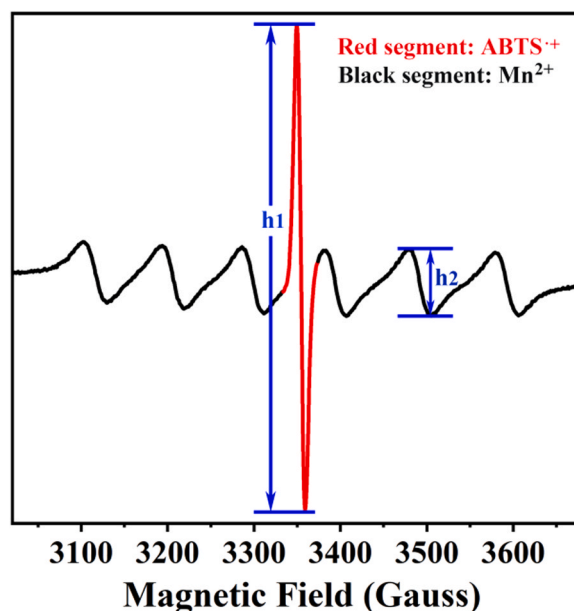In Figs. 3b and 3c, MnO$_2$ concentration was set at 0.005 mg mL^{-1} (i.

Fig. 4. Signals of ABTS$^{\bullet+}$ and Mn^{2+} coexisting in an ESR spectrum. Red line segment represents the signal of ABTS$^{\bullet+}$; black line segment represents the signal of Mn^{2+}.

e. 0.06 mmol L^{-1}) and ABTS concentration was increased from 0 to 5 mmol L^{-1}. Fig. 3b shows that ESR signal of Mn^{2+} appeared only when ABTS was added into the system. That is to say, there was no signal of Mn^{2+} when there was only dissolved oxygen and no ABTS. Thus the generation of Mn^{2+} must be caused by the redox reaction between MnO$_2$ nanosheets and ABTS. The signal of Mn^{2+} stopped increasing at ABTS concentration higher than 0.625 mmol L^{-1}, illustrating a complete consumption of MnO$_2$ by the redox reaction. However, the signal of ABTS$^{\bullet+}$ continued to increase when ABTS concentration increased from 0.625 to 1.25 mmol L^{-1} and no more Mn^{2+} emerged in this interval. Thus besides the redox reaction, there should be ROS effect existing in the system at the same time. By calculation according to Fig. 3c and Figure S3, in the presence of 2.5 mmol L^{-1} ABTS, approximately 0.8 mmol L^{-1} ABTS was oxidized to ABTS$^{\bullet+}$. Among the total amount (0.8 mmol L^{-1}) of oxidized ABTS, only 0.12 mmol L^{-1} ABTS was oxidized by the redox reaction based on the fact that one molecule of MnO$_2$ oxidizes two molecules of ABTS. Most ABTS was oxidized to ABTS$^{\bullet+}$ by O$_2^{\bullet-}$ generated from MnO$_2$ nanosheet's catalysis as oxidase mimic. Consequently, this study demonstrates the coexistence of redox reaction and oxidase-mimic activity of MnO$_2$ nanosheet in the presence of ABTS, and the dominant contribution for the oxidation of ABTS comes from the role of nanozyme.

The contribution of O$_2^{\bullet-}$ for the oxidation of ABTS was further proved by adding benzoquinone which is a scavenger of O$_2^{\bullet-}$ in the reaction system and the results are displayed in Figs. 3b, 3c and 3d. In the presence of benzoquinone, the signal of Mn^{2+} did not change whereas the signal of ABTS$^{\bullet+}$ dramatically declined, verifying that O$_2^{\bullet-}$ was an important cause for the oxidation of ABTS.

3.4. Calculation of the ESR signal ratio of ABTS$^{\bullet+}$ to Mn^{2+}

Both Mn^{2+} and ABTS$^{\bullet+}$ have single electrons, so both are paramagnetic and present good ESR signals. Fig. 4 displays the ESR spectrum composed of both signals. In aqueous solution, the ESR signal of Mn^{2+} (Fig. 4, black line segment) consists of six split peaks with adjacent peaks spaced approximately 95 Gauss apart [33]. The ESR signal of ABTS$^{\bullet+}$ (Fig. 4, red line segment) had only one peak located in the middle of the spectrum. When these two signals coexisted in a spectrum, they basically did not overlap with each other. The value for the peak height of ABTS$^{\bullet+}$
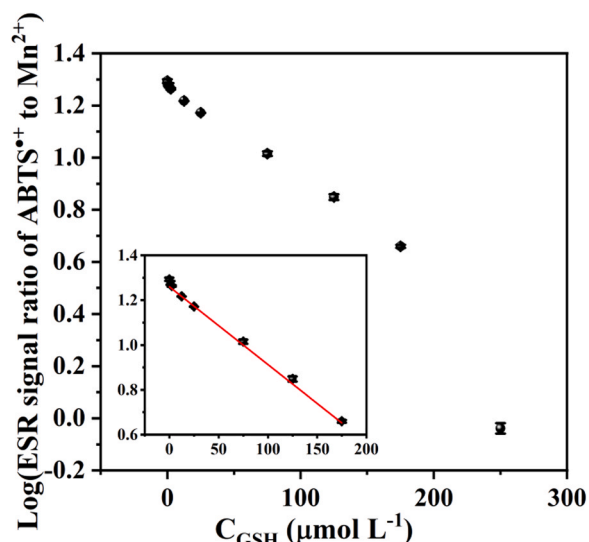
Fig. 5. Logarithm of ESR signal ratio of ABTS$^{\bullet+}$ to Mn^{2+} vs. GSH concentration (Inset shows a linear fit in the range of 0–175 µmol L^{-1}). The error bar represents SD.

Table 1

Comparison of different methods for GSH detection.

Method	Material	Linear range (µmol L^{-1})	LOD (µmol L^{-1})	Ref.
Fluorometric	Cdots@MnO$_2$ nanocomposite	15–200	15	[40]
Fluorometric	Go-MnO$_2$-FL	10–2000	1.53	[5]
Colorimetry	Co$_3$O$_4$/BiPc (OC$_8$H$_9$)$_{12}$	10–200	4	[41]
Colorimetry	PSMOF	1–20	0.68	[42]
Colorimetry	COF-300-AR	1–15	1.0	[43]
Colorimetry	Co$_3$O$_4$-MMT+TM	0.1–20	0.088	[44]
Colorimetry	Fe$_3$O$_4$ NPs	3–30	3.0	[45]
Lateral flow plasmonic biosensor	AuVCs	25–500	9.8	[46]
ESR	MnO$_2$ nanosheets	0.6–175	0.18	This work

signal was measured and set as "h1". The height value for the 5th peak of Mn^{2+} was measured and set as "h2". The ratio of h1/h2 was calculated and set as the ESR signal ratio of ABTS$^{\bullet+}$ to Mn^{2+}, which was used in the optimization of experimental conditions and construction of standard curve.

3.5. Sensing mechanism for GSH detection

When there was no GSH in the reaction system, MnO$_2$ nanozyme produced O$_2^{\bullet-}$ through catalysis and then O$_2^{\bullet-}$ oxidized ABTS to form ABTS$^{\bullet+}$. On the other hand, in the presence of ABTS, a portion of MnO$_2$ was reduced by ABTS through redox reaction and yielded some Mn^{2+}. When GSH was added, MnO$_2$ underwent redox reaction with GSH to produce more Mn^{2+} and the height of ESR signal of Mn^{2+} increased. When GSH concentration gradually increased, MnO$_2$ nanosheets were directly consumed, the oxidation of ABTS was greatly suppressed and correspondingly the yield of ABTS$^{\bullet+}$ decreased rapidly. Therefore, as the concentration of GSH increased, the ESR signal of ABTS$^{\bullet+}$ descended and on the contrary the ESR signal of Mn^{2+} ascended. Accordingly, the signal ratio of ABTS$^{\bullet+}$ to Mn^{2+} was proportional to the concentration of GSH, so a standard curve could be established.

3.6. Analytical performances for the GSH assay

In order to obtain optimal GSH detection performance, several experimental parameters were optimized including MnO$_2$ concentration, ABTS concentration, reaction time and reaction pH, as shown in Figure S4. Under the optimal experimental conditions, a series of ESR spectra at varied GSH concentrations from 0 to 250 µmol L^{-1} were collected. Taking GSH concentration as the abscissa and the logarithmic value of the signal ratio of ABTS$^{\bullet+}$ to Mn^{2+} as the ordinate, the standard curve was constructed in Fig. 5. The signal ratio logarithm decreased linearly at GSH concentration from 0 to 175 µmol L^{-1}, and this part of the curve was fitted using a linear equation, as seen in the inset of Fig. 5. The linear regression equation was Log(ESR signal ratio of ABTS$^{\bullet+}$ to Mn^{2+})=1.2608($\pm$0.0024)−0.0035($\pm$0.0001)[GSH] with a linear correlation coefficient of 0.998. The limit of detection (LOD) for GSH was calculated to be 0.18 µmol L^{-1} based on the formula LOD=3 SD/slope (n=7).

In order to prove that the proposed ratiometric probe could improve the sensitivity of detection compared to the method measuring only

single signal, the UV–vis absorbance of ABTS$^{\bullet+}$ was determined and the standard curve was established in Figure S5a. The LOD was calculated to be 2.04 µmol L^{-1} which was 11.3 times higher than that of ratiometric probe. In addition, a standard curve of ABTS$^{\bullet+}$ ESR signal vs. GSH concentration was plotted in Figure S5b and the LOD was found to be 1.49 µmol L^{-1} which was 8.3 times higher than that of ratiometric probe. These comparisons demonstrated that the design of ratiometric probe could improve the sensitivity of detection.

The comparison of the analytical performance (LOD and linear range) of this work with other reported GSH assays is listed in Table 1. The LODs of the reported methods listed in the table are between 0.088 and 15 µmol L^{-1}, while the LOD of this work was low to 0.18 µmol L^{-1}, and therefore a satisfactory detection limit of the present method was obtained. The linear range of most methods in the table is between 1 and 2 orders of magnitude, while the linear range of this work (0.6–175 µmol L^{-1}) exceeded 2 orders of magnitude. The content of GSH in different biological samples differs widely, e.g. GSH in erythrocyte cells is 1192 µmol L^{-1} whereas GSH in plasma is only 6.27 µmol L^{-1} found by Mills et al. [34]. Therefore the proposed method with wider linear range would be more promising in real biological sample analysis. Moreover, the present method is very simple with no requirement of heating and long incubation time.

3.7. Interference studies

To further evaluate the selectivity and specificity of the proposed method, we investigated the effects of 10 kinds of biologically relevant substances on GSH detection, including K$^+$, Mg^{2+}, Na$^+$, glucose (Glu), glycine (Gly), leucine (Leu) and arginine (Arg) at 0.25 mmol L^{-1}, as well as ascorbic acid (AA), L-cysteine (Cys) and homocysteine (Hcy) at 0.175 mmol L^{-1}. Figure S6 indicates that most substances had no significant effect on the detection of GSH expect for three reducing agents including AA, Cys and Hcy. However, the concentrations of AA, Cys and Hcy were much lower than that of GSH in biological systems [12,35] including human erythrocytes [36,37]. For example, in human erythrocytes, the concentrations of AA, Cys and Hcy are respectively 45, 5.8 and 0.95 µmol L^{-1} [36,37], and interference from these three agents was negligible when detecting GSH in the range of 0.46–2.21 mmol L^{-1} in human erythrocytes [38]. Consequently, interference studies proved that the present method had good selectivity and anti-interference capability.

3.8. Detection of GSH in human erythrocyte cells

The proposed method was applied to the detection of GSH in human erythrocyte cells. The content of GSH in the analytical sample was found to be 30.14$\pm$1.24 µmol L^{-1}, which was consistent with the value (35.18

Table 2
Detection of GSH in human erythrocyte cells.

Sample	Detected (μmol L^{-1})	Added (μmol L^{-1})	Total found (μmol L^{-1})	Recovery (%)	RSD (%, n=3)
Erythrocyte	30.14 ± 1.24	25.00	53.13 ± 1.61	92.0	7.0
		37.50	64.86 ± 1.02	92.6	4.4
		50.00	75.59 ± 0.57	90.9	2.5

±0.56 μmol L^{-1}) obtained by the traditional Ellman method. The result of the analytical sample corresponded to a GSH concentration of 964.55 ±39.78 μmol L^{-1} in erythrocyte cells. In whole blood, >99 % GSH is in erythrocyte cells [39]. GSH concentration in human erythrocytes is reported to be 0.46–2.21 mmol L^{-1} in previous publications [38] and our result was within this range. The analytical sample was spiked respectively with three concentrations (25.00, 37.50 and 50.00 μmol L^{-1}) of GSH. The results are listed in Table 2 and the recoveries of GSH ranged from 90.9 % and 92.6 %. The satisfactory results indicated that the proposed method was accurate and effective for GSH detection in real samples.

4. Conclusion

In this work, oxidase-like MnO$_2$ nanosheets with good affinity for substrate ABTS and excellent catalytic ability were synthesized. Based on the stable ESR signal of ABTS$^{\bullet+}$ and Mn^{2+}, GSH was detected by measuring the signal ratio of ABTS$^{\bullet+}$ to Mn^{2+}. To measure the signal ratio instead of single signal could reduce the influence from the background signal and help improve the accuracy and sensitivity of detection. The method presented high sensitivity for GSH detection with a LOD of 0.18 μmol L^{-1}. Moreover, simultaneous monitoring of the changes happen to both nanozyme and its substrate would deepen the understanding of the mechanism for the interaction between nanomaterial and its chromogenic substrate.

CRediT authorship contribution statement

Zhimin Zhang: Data curation. **Meijun Lu:** Data curation. **Chunyu Wang:** Investigation, Data curation. **Daqian Song:** Supervision, Resources, Project administration. **Ziwei Zhang:** Writing – review & editing, Software, Project administration, Data curation, Conceptualization. **Hui Shi:** Writing – original draft, Validation, Investigation, Data curation, Conceptualization. **Li Tang:** Writing – original draft, Validation, Investigation, Data curation, Conceptualization.

Declaration of Competing Interest

The authors declare that they have no known competing financial interests or personal relationships that could have appeared to influence the work reported in this paper.

Data Availability

Data will be made available on request.

Appendix A. Supporting information

Supplementary data associated with this article can be found in the online version at doi:10.1016/j.snb.2024.136112.

References

[1] Á. Sánchez-Illana, F. Mayr, D. Cuesta-García, J.D. Piñeiro-Ramos, A. Cantarero, Mdl Guardia, et al., On-capillary surface-enhanced Raman spectroscopy: determination of glutathione in whole blood microsamples, Anal. Chem. 90 (2018) 9093–9100.

[2] A. Pompella, A. Visvikis, A. Paolicchi, V.D. Tata, A.F. Casini, The changing faces of glutathione, a cellular protagonist, Biochem. Pharmacol. 66 (2003) 1499–1503.

[3] J. Yin, Y. Kwon, D. Kim, D. Lee, G. Kim, Y. Hu, et al., Cyanine-based fluorescent probe for highly selective detection of glutathione in cell cultures and live mouse tissues, J. Am. Chem. Soc. 136 (2014) 5351–5358.

[4] G.P. McDermott, P.S. Francis, K.J. Holt, K.L. Scott, S.D. Martin, N. Stupka, et al., Determination of intracellular glutathione and glutathione disulfide using high performance liquid chromatography with acidic potassium permanganate chemiluminescence detection, Analyst 136 (2011) 2578–2585.

[5] Y. Guo, X. Zhang, F.-G. Wu, A graphene oxide-based switch-on fluorescent probe for glutathione detection and cancer diagnosis, J. Colloid Interface Sci. 530 (2018) 511–520.

[6] A. Gupta, N.C. Verma, S. Khan, C.K. Nandi, Carbon dots for naked eye colorimetric ultrasensitive arsenic and glutathione detection, Biosens. Bioelectron. 81 (2016) 465–472.

[7] J. Vacek, B. Klejdus, J. Petrlová, L. Lojková, V. Kubáň, A hydrophilic interaction chromatography coupled to a mass spectrometry for the determination of glutathione in plant somatic embryos, Analyst 131 (2006) 1167–1174.

[8] B. Bayram, G. Rimbach, J. Frank, T. Esatbeyoglu, Rapid method for glutathione quantitation using high-performance liquid chromatography with coulometric electrochemical detection, J. Agric. Food Chem. 62 (2013) 402–408.

[9] M. Liang, X. Yan, Nanozymes: from new concepts, mechanisms, and standards to applications, Acc. Chem. Res. 52 (2019) 2190–2200.

[10] J. Wu, X. Wang, Q. Wang, Z. Lou, S. Li, Y. Zhu, et al., Nanomaterials with enzyme-like characteristics (nanozymes): next-generation artificial enzymes (II), Chem. Soc. Rev. 48 (2019) 1004–1076.

[11] R.D. Isho, N.M. Sher Mohammad, K.M. Omer, Synthesis of MnO$_2$ sub-microspheres with effective oxidase-mimicking nanozymes for the colorimetric assay of ascorbic acid in orange fruits and juice, N. J. Chem. 47 (2023) 7800–7809.

[12] J. Liu, L. Meng, Z. Fei, P.J. Dyson, X. Jing, X. Liu, MnO$_2$ nanosheets as an artificial enzyme to mimic oxidase for rapid and sensitive detection of glutathione, Biosens. Bioelectron. 90 (2017) 69–74.

[13] A. Floegel, D.O. Kim, S.J. Chung, S.I. Koo, O.K. Chun, Comparison of ABTS/DPPH assays to measure antioxidant capacity in popular antioxidant-rich US foods, J. Food Compos Anal. 24 (2011) 1043–1048.

[14] Y. Huang, J. Lin, J. Zou, J. Xu, M. Wang, H. Cai, et al., ABTS as an electron shuttle to accelerate the degradation of diclofenac with horseradish peroxidase-catalyzed hydrogen peroxide oxidation, Sci. Total Environ. 798 (2021) 149276.

[15] S. Tian, X. Li, J. Jiang, L. Tang, H. Zhang, Y. Yu, et al., Highly sensitive detection of rabbit IgG by electron spin resonance using CuS nanoparticles as probe, Sens. Actuator B Chem. 338 (2021) 129835.

[16] L. Tang, C. Wang, S. Tian, Z. Zhang, Y. Yu, D. Song, et al., Label-free and ultrasensitive detection of butyrylcholinesterase and organophosphorus pesticides by Mn(II)-based electron spin resonance spectroscopy with a zero background signal, Anal. Chem. 94 (2022) 16189–16195.

[17] K. Kai, Y. Yoshida, H. Kageyama, G. Saito, T. Ishigaki, Y. Furukawa, et al., Room-temperature synthesis of manganese oxide monosheets, J. Am. Chem. Soc. 130 (2008) 15938–15943.

[18] Y. Lin, Q. Zhou, D. Tang, R. Niessner, D. Knopp, Signal-on photoelectrochemical immunoassay for aflatoxin B1 based on enzymatic product-etching MnO$_2$ nanosheets for dissociation of carbon dots, Anal. Chem. 89 (2017) 5637–5645.

[19] C. Yao, J. Wang, A. Zheng, L. Wu, X. Zhang, X. Liu, A fluorescence sensing platform with the MnO$_2$ nanosheets as an effective oxidant for glutathione detection, Sens. Actuator B Chem. 252 (2017) 30–36.

[20] Z. Zhao, H. Fan, G. Zhou, H. Bai, H. Liang, R. Wang, et al., Activatable fluorescence/MRI bimodal platform for tumor cell imaging via MnO$_2$ nanosheet–aptamer nanoprobe, J. Am. Chem. Soc. 136 (2014) 11220–11223.

[21] R. Re, N. Pellegrini, A. Proteggente, A. Pannala, M. Yang, C. Rice-Evans, Antioxidant activity applying an improved ABTS radical cation decolorization assay, Free Radic. Biol. Med. 26 (1999) 1231–1237.

[22] H. Liang, F. Lin, Z. Zhang, B. Liu, S. Jiang, Q. Yuan, et al., Multicopper laccase mimicking nanozymes with nucleotides as ligands, ACS Appl. Mater. Interfaces 9 (2017) 1352–1360.

[23] Y. Gao, X. Gao, H. Hou, Z. Qu, H. Li, B.J. Du, et al., Stabilizer-free MnO$_2$ nanozyme with singlet-oxygen conducted high oxidase-like activity and fast catalysis capability for improving alkaline phosphatase assay, Sens. Actuator B Chem. 404 (2024) 135280.

[24] H. Noda, K. Oikawa, H. Ohya-Nishiguchi, H. Kamada, Detection of superoxide ions from photoexcited semiconductors in non-aqueous solvents using the ESR spin-trapping technique, Bull. Chem. Soc. Jpn. 66 (1993) 3542–3547.

[25] G.R. Buettner, Spin trapping: ESR parameters of spin adducts, Free Radic. Biol. Med 3 (1987) 259–303.

[26] R. Konaka, E. Kasahara, W.C. Dunlap, Y. Yamamoto, K.C. Chien, M. Inoue, Irradiation of titanium dioxide generates both singlet oxygen and superoxide anion, Free Radic. Biol. Med. 27 (1999) 294–300.

[27] Y. Zhao, Y. Zhang, X. Liang, D.-P. Yang, L. Han, The influence of substrates addition order on colorimetric assay based on MnO$_2$ nanocubes: a novel turn-off H$_2$O$_2$ assay strategy in water-soak foods, Food Chem. 419 (2023) 136059.

[28] P. Ni, X. Wei, J. Guo, X. Ye, S. Yang, On the origin of the oxidizing ability of ceria nanoparticles, RSC Adv. 5 (2015) 97512–97519.

[29] Y. He, Z. Wang, D. Long, Direct visual detection of MnO_2 nanosheets within seconds, Anal. Bioanal. Chem. 408 (2016) 1231–1236.

[30] J. Ge, R. Cai, X. Chen, Q. Wu, L. Zhang, Y. Jiang, et al., Facile approach to prepare HSA-templated MnO_2 nanosheets as oxidase mimic for colorimetric detection of glutathione, Talanta 195 (2019) 40–45.

[31] L. Tian, Z. Huang, W. Na, Y. Liu, S. Wang, Y. He, et al., Heterojunction MnO_2-nanosheet-decorated Ag nanowires with enhanced oxidase-like activity for the sensitive dual-mode detection of glutathione, Nanoscale 14 (2022) 15340–15347.

[32] J. Wang, Q. Lu, C. Weng, X. Li, X. Yan, W. Yang, et al., Label-free colorimetric detection of acid phosphatase and screening of its inhibitors based on biomimetic oxidase activity of MnO_2 nanosheets, ACS Biomater. Sci. Eng. 6 (2020) 3132–3138.

[33] R. Carpenter, Quantitative electron spin resonance (ESR) determinations of forms and total amounts of Mn in aqueous environmental samples, Geochim. Cosmochim. Acta 47 (1983) 875–885.

[34] B.J. Mills, C.A. Lang, Differential distribution of free and bound glutathione and cyst(e)ine in human blood, Biochem. Pharmacol. 52 (1996) 401–406.

[35] S. Li, L. Wang, X. Zhang, H. Chai, Y. Huang, A Co,N co-doped hierarchically porous carbon hybrid as a highly efficient oxidase mimetic for glutathione detection, Sens Actuator B Chem. 264 (2018) 312–319.

[36] D. Giustarini, A. Milzani, I. Dalle-Donne, R. Rossi, Red blood cells as a physiological source of glutathione for extracellular fluids, Blood Cells Mol. Dis. 40 (2008) 174–179.

[37] S.J. Padayatty, M. Levine, Vitamin C: the known and the unknown and Goldilocks, Oral. Dis. 22 (2016) 463–493.

[38] C.-W. Chen, F.-Y. Liao, Y.-C. Lin, T.-J. Hsieh, J.-R. Weng, C.-H. Feng, Microwave-assisted derivatization combined with coacervative extraction for determining glutathione in biomatrix samples, followed by capillary liquid chromatography, Talanta 199 (2019) 464–471.

[39] Y. Hou, J.C. Ndamanisha, L. Guo, X. Peng, J. Bai, Synthesis of ordered mesoporous carbon/cobalt oxide nanocomposite for determination of glutathione, Electro Acta 54 (2009) 6166–6171.

[40] N. Sohal, B. Maity, S. Basu, Carbon dot–MnO_2 nanosphere composite sensors for selective detection of glutathione, ACS Appl. Mater. Interfaces 3 (2020) 5955–5964.

[41] X. Kong, R. Yang, Y. Li, Y. Wei, Y. Sun, H. Lyu, et al., Co_3O_4-binuclear phthalocyanine nanocomposites with enhanced peroxidase-like activity for sensitive detection of glutathione, Colloid Surf. A Physicochem Eng. Asp. 615 (2021) 126261.

[42] Y. Liu, M. Zhou, W. Cao, X. Wang, Q. Wang, S. Li, et al., Light-responsive metal–organic framework as an oxidase mimic for cellular glutathione detection, Anal. Chem. 91 (2019) 8170–8175.

[43] P. Jin, X. Niu, F. Zhang, K. Dong, H. Dai, H. Zhang, et al., Stable and reusable light-responsive reduced covalent organic framework (COF-300-AR) as a oxidase-mimicking catalyst for GSH detection in cell lysate, ACS Appl. Mater. Interfaces 12 (2020) 20414–20422.

[44] Y. Gao, K. Wu, H. Li, W. Chen, M. Fu, K. Yue, et al., Glutathione detection based on peroxidase-like activity of Co_3O_4–montmorillonite nanocomposites, Sens Actuator B Chem. 273 (2018) 1635–1639.

[45] Y. Ma, Z. Zhang, C. Ren, G. Liu, X. Chen, A novel colorimetric determination of reduced glutathione in A549 cells based on Fe3O4 magnetic nanoparticles as peroxidase mimetics, Analyst 137 (2012) 485–489.

[46] H.-H. Pang, Y.-C. Ke, N.-S. Li, Y.-T. Chen, C.-Y. Huang, K.-C. Wei, et al., A new lateral flow plasmonic biosensor based on gold-viral biomineralized nanozyme for on-site intracellular glutathione detection to evaluate drug-resistance level, Biosens. Bioelectron. 165 (2020) 112325.

Hui Shi is pursuing her Master degree in College of Chemistry, Jilin University. Her interest is spectral analysis and electron spin resonance spectroscopy.

Li Tang received her master's degree in College of Chemistry, Jilin University. Her interest is spectral analysis and electron spin resonance spectroscopy.

Chunyu Wang is currently a professor in State Key Laboratory of Supramolecular Structure and Materials, Jilin University. His research interest focuses on nuclear magnetic resonance and electron spin resonance spectroscopies.

Zhimin Zhang is pursuing her Master degree in College of Chemistry, Jilin University. Her interest is spectral analysis.

Meijun Lu is pursuing her Master degree in College of Chemistry, Jilin University. Her interest is spectral analysis and electron spin resonance spectroscopy.

Daqian Song gained his doctor's degree from College of Chemistry, Jilin University in 2003 and he is a professor in that school. His research areas are spectral and chromatography analysis.

Ziwei Zhang received his PhD degree in biophysics in Cornell University in 2010. She is currently an associate professor in Jilin University. Her research interest focuses on spectral analysis and electron spin resonance spectroscopy.